Journal of Controlled Release
Regular article

Vascular-targeted nanotherapy for obesity: unexpected passive targeting mechanism to obese fat for the enhancement of active drug delivery

Md. Nazir Hossen[a], Kazuaki Kajimoto[a], Hidetaka Akita[b], Mamoru Hyodo[a], Hideyoshi Harashima[a, b,*]

[a]Laboratory of Innovative Nanomedicine, Faculty of Pharmaceutical Sciences, Hokkaido University, Kita 12, Nishi 6, Kita-ku, Sapporo, Hokkaido 060-0812, Japan
[b]Laboratory for Molecular Design of Pharmaceutics, Faculty of Pharmaceutical Sciences, Hokkaido University, Kita 12, Nishi 6, Kita-ku, Sapporo, Hokkaido 060-0812, Japan

*Correspondence to:
Hideyoshi Harashima, Ph.D.
Laboratory for Molecular Design of Pharmaceutics,
Faculty of Pharmaceutical Sciences, Hokkaido University
Kita-12, Nishi-6, Kita-ku, Sapporo, Hokkaido 060-0812, Japan
Tel: +81-11-706-3919
Fax: +81-11-706-4879
E-mail: harasima@pharm.hokudai.ac.jp

Abstract:
We previously reported that nanoparticles (NPs) modified with a prohibitin-homing peptide ligand via a short PEG_{2kDa}-spacer could deliver its pay-load into the cytoplasm of endothelial cells in murine adipose tissue and escape from endosomes/lysosomes *in vitro*. We herein report, for the first time, on a dual-targeting strategy for mediating the enhanced targeting activity of NPs to adipose endothelial cells in diet-induced obesity (DIO). The targeted accumulation of prohibitin-targeted nanoparticles (PTNP), modified with a peptide ligand via a long PEG-linker, was significantly increased in white fat vessels of normal healthy mice compared to the other non-PEGylated targeted NPs, whereas the undesired accumulation of PTNP in the liver was considerably reduced. These results demonstrate that the PEGylation of targeted NPs is a critical factor in maximizing the *in vivo* targeted delivery of NPs and can be attributed to a significant decrease in recognition by the reticuloendothelial system. After systemic administration to DIO mice, PTNP exclusively accumulated in both adipose vessels and angiogenic clusters of obese fat cells. Surprisingly, PEGylated NPs with no active targeting moieties also accumulated in these clusters, demonstrating that the nanoscaled carriers passively accumulate in clusters via a mechanism similar to that for the enhanced permeability and retention effect, as has been well established in tumor targeting. Therefore, the enhanced delivery of PTNP appears to be mediated by both passive accumulation to angiogenic regions and active recognition by endothelial cells. Thus, the systemic administration of a proapoptotic peptide with the delivery via PTNP significantly reduced the body weight of DIO mice, as evidenced by the targeted ablation of adipose endothelial cells. These findings are potentially useful in terms of the design and development of vascular-targeted nanotherapy in the effective control of obesity.

Key Words:
Active targeting, passive targeting, vascular-targeted nanoparticle, anti-angiogenesis, obesity

1. Introduction

A growing demand in developed societies worldwide exists for an effective and safe therapy for the management of obesity. The only remaining FDA-approved anti-obesity drug is Orlistat, a lipase inhibitor that acts in the gastrointestinal tract (GIT), but it is also associated with numerous side effects, including severe diarrhea and nephrotoxicity. One potential alternative approach to obesity control is the targeting of endothelial cells in white fat vessels (WFV). Whilst endothelial cells that form the walls of WFV provide the oxygen and nutrients needed for the survival and growth of resident cells including parenchymal adipocytes to be stored for energy for a long period as triglycerides from the circulation, these cells therefore represent an attractive target for obesity therapy. Moreover, new blood vessel growth (angiogenesis) in WF may simultaneously be associated with the growth of adipocytes (adipogenesis) and subsequently result in an increase in WF mass through the process of angiogenesis-dependent adipogenesis [1, 2]. Findings reported in several studies indicate that the use of a non-specific angiogenic inhibitor (TNP-470) that functions via apoptosis/necrosis of endothelial cells in WF may be useful in terms of controlling obesity [3, 4], but their large volume of distribution after *i.v*-administration, which is crucial for them to be effective resulted in a narrow therapeutic index with an undesirable toxicity in healthy tissues [5]. Thus, an unmet need exists to develop an effective, safe and better-tolerated obesity therapy.

For the development of targeted therapy in obesity, Kolonin, *et al*. reported that a small peptide (CKGGRAKDC) is able to specifically bind to prohibitin, located on the endothelial cell-surface in WFV [6], and was subsequently fused with a cell death-inducing peptide (D(KLAKLAK)2, KLA) [7]. The subcutaneous injection of the peptidomimetic CKGGRAKDC-GG-$_{D}$(KLAKLAK)$_2$, referred to as an Adipotide [8], was reported to promote weight loss in obese mice [6], rats [9] and rhesus monkeys [8]. The U.S. Food and Drug Administration (FDA) recently approved the initiation of Phase I clinical trials to evaluate the safety of Adipotide. However, for effective obesity control using Adipotide, frequent administration (daily) via subcutaneous injection was necessary in their animal examinations [6, 8, 9]. Therefore, the technological evolution of the promising strategy of targeted antiangiogenic therapy may be required for the global acceleration of the drug discovery and development in obesity and metabolic disorders.

We recently reported on the development of an *in vitro* adipose endothelial cell targeted nanoparticle (NP) [10] utilizing a WFV-targeting peptide ligand (KGGRAKD) [6]. The preparation was a liposomal NP composed of biocompatible lipids with its surface modified with a linear peptide containing a WFV-targeting motif, attached via a polyethylene glycol (PEG) spacer. In a previous study, we reported that the targeted NP specifically delivered encapsulated compounds to the cytoplasm of primary cultured endothelial cells derived from murine adipose tissue [11] through their uptake by prohibitin-mediated endocytosis [10].

The goal of this study was to establish a potential adipose endothelial cell-targeted NP that could be used for the *in vivo* systemic delivery of therapeutics. Furthermore, in an evaluation of the targeted delivery of NPs to WFV in a mouse model of diet-induced obesity (DIO), we discovered an unexpected mechanistic advantage of nanoparticle-based delivery, in that the targeted delivery of nanoscaled carriers into the angiogenic region of obese adipose tissue could be passively promoted via a physical property (enhanced permeability) of a discontinuous architecture in angiogenic vessels. In addition, systemic delivery of the proapoptotic peptide through vascular-targeted NPs successfully reduced the body weight of DIO mice. On the basis of the present findings, we propose herein a novel concept for vascular-targeted nanotherapy in which antiangiogenesis is integrated with nanotechnology.

2. Materials and methods

2.1. Animals and reagents

Male C57BL/6J-DIO mice (body weight >38g) obtained from The Charles River Laboratories Japan (Yokohama, Japan) or five week old male *wt* C57BL/6J mice were purchased from SLC Japan (Shizuoka, Japan). The mice were housed in standard mouse cages with a 12h light/12h dark cycle at 23°C. All animals were acclimatized for one week prior to use. Animal experiments involved standard procedures approved by the institutional animal care and research advisory committee of Hokkaido University, Sapporo, Japan.

PEG_{5kDa}-DSPE and PEG_{2kDa}-DSPE with a functional maleimide (Mal) moiety at the terminal end of PEG: N-[(3-maleimide-1-oxopropyl) aminopropyl polyethylene glycolcarbamyl] distearoyl-sn-Glycero-3-phosphoethanolamine were purchased from Nippon Oil and Fat Co. (Tokyo, Japan). 1,2 dioleolyl-sn-glycero-3-phosphoethanolamine-N-(lissamine rhodamine B sulfonyl) (Rhodamine-DOPE) or 1,2-dioleoyl-*sn*-glycero-3-phosphoethanolamine-N-(7-nitro-2-1,3-benzoxadiazol-4-yl) (NBD-DOPE) were obtained from Avanti Polar Lipids (Alabaster, AL, USA). Peptides (GKGGRAKDGGC and $_D(KLAKLAK)_2$) were synthesized by Toray Industries Inc. (Tokyo, Japan). These peptides were purified by high-performance liquid chromatography to >95% purity.

2.2. Synthesis of targeting peptide-modified PEG-lipid

We conjugated a prohibitin-targeted peptide (GKGGRAKDGGC-SH) with Mal-PEG_{5kDa}-DSPE as described previously [10]. Briefly, GKGGRAKDGGC-SH and Mal-PEG_{5kDa}-DSPE were dissolved in separate portions of distilled water. For the complete dissolution of DSPE-PEG_{5kDa}-Mal, bath sonication was utilized. GKGGRAKDGGC-S-PEG_{5kDa}-DSPE (5 mM) was prepared by incubating a 1:1 (molar ratio) mixture of the Mal-PEG_{5kDa}-DSPE solution (10 mM) and the GKGGRAKDGGC-SH (10 mM) for 24h at 30°C with continuous shaking on a Bio-shaker. The conjugation of peptide to PEG-lipid was confirmed by MALDI-TOF MS spectrometry as previously described [10] (data not shown). To determine the conjugation efficiency of the peptide and Mal-PEG_{5KDa}-DSPE, GKGGRAKDGGC-SH and Mal-PEG_{5kDa}-DSPE were further separately dissolved in deuterium oxide (D_2O), prepared as previously described and then analyzed by ^{1}HNMR (ECA500, JEOL, Japan) at 500 MHz. The chemical shifts of the ^{1}H NMR spectra are denoted in ppm (parts per million) where H_2O was used as an internal standard (4.73 ppm). The efficiency of this reaction was estimated from three sets of NMR results. The signal of methine proton bound to Mal group is known to be found at 6.7 ppm (SDBSWeb: http://riodb01.ibase.aist.go.jp/sdbs/ (National Institute of Advanced Industrial Science and Technology)) and it was also clearly detected in the spectrum of Mal-PEG_{5kDa}-DSPE (**Fig. S1B**). No overlapping signals at 6.7 ppm were observed in the case of peptide (**Fig. S1A)**. The Mal signal at 6.7 ppm completely disappeared in the spectrum of desired conjugate compound (**Fig.S1C**, GKGGRAKDGGC-S-PEG_{5kDa}-DSPE) due to the conversion from double bond to single bond of maleimide ring through the Micheal type addition of the peptide-SH and Mal-PEG_{5KDa}-DSPE. From these results, it was concluded that all maleimide groups had reacted with peptide-SH groups, so we concluded that the reaction efficiency was essentially 100%.

2.3. Nanoparticle preparation and characterization

Egg york phosphatidylcholine and cholesterol based-nanoparticles in which a prohibitin targeting peptide-conjugated PEG-lipid (Pep-PEG_{5kDa}-DSPE), PEG_{5kDa}-DSPE, PEG_{2kDa}-DSPE were incorporated on the surface with the following compositions; 1.25 mol% Pep-PEG_{5kDa}-DSPE and 1 mol% PEG_{2kDa}-DSPE of total lipids for PTNP, 1.25 mol% PEG_{5kDa}-DSPE and 1 mol% PEG_{2kDa}-DSPE of total lipids for NTNP, 1 or 10 mol% PEG_{2KDa}-DSPE of total lipids for low or high density PEGylated NPs, respectively, and the aqueous phase with the synthesized KLA peptide or rhodamine were prepared by a previously

described reverse phase evaporation (REV) method [10, 12]. For the preparation of fluorescent-labeled PTNP or NTNP, rhodamine-DOPE or NBD-DOPE were added at 1 mol% of total lipids. 125 μM of KLA was applied to prepare the KLA-PTNP. To remove free KLA or free rhodamine, the samples were subjected to 2 ultracentrifugations of 30 min each at 82000x g for each washing. The sizes and zeta potentials of NPs were measured by photon correlation spectroscopy on a Malvern Zetasizer (Malvern instruments, Malvern, UK). The physicochemical characteristics of NPs utilized in this study are summarized in **Table 1**.

5-Carboxyfluorescein (FAM)-labeled KLA (AnaSpec) was utilized to determine the encapsulation of the KLA peptide. After ultracentrifugation, the supernatants were removed by aspiration and pellets containing FAM-labeled KLA or rhodamine-loaded nanoparticles were dispersed in 10 mM HEPES. The fluorescent intensity (FI) of the samples and controls (empty-PTNP or HEPES) as a blank was measured at the FAM or the rhodamine fluorescence intensity using a FP-750 Spectro-fluorometer (JAS Co, Tokyo, Japan). We measured the recovery ratio of encapsulated KLA or rhodamine according to the following formula: the Recovery Ratio (%) = P1 / P0 × 100, Where P0= FI of the total KLA or rhodamine used in nanoparticle (free + encapsulated), P1= FI of KLA or rhodamine (encapsulated). The recovery ratio of KLA and rhodamine was 9.4 ± 3.4 and 2.8 ± 0.5%, respectively.

2.4. Homing of nanoparticles to blood vessels via three dimensional confocal observation

The observation of living adipose tissue was performed as described in a previous report [2] with minor modifications. Briefly, mice (6-wk-old male C57BL/6J or DIO C57BL/6J mice (>42g)) were intravenously administered the NPs labeled with rhodamine-DOPE or NBD-DOPE to a lipid dose of 0.1 mmol/kg. For a comparable study of targeted delivery between ligand peptide and nanoparticles, mice were *i.v*-injected with rhodamine-loaded NPs (PTNP or NTNP) or rhodamine-conjugated ligand peptide at a rhodamine dosage of 0.2 μmol/kg. The Recovery Ratio of rhodamine (2.8 ± 0.5%) encapsulated into nanoparticles was taken into account in the dose calculation. To visualize blood vessels, a FITC- or Alexa647-*Griffonia simplicifolia* isolectin (GSIB4) was injected intravenously (50 μg/mice) 30 min prior to tissue collection. The mice were anesthetized and as much blood as possible removed by cardiac puncture. Tissues from the adipose inguinal and epididymal regions, brain, heart, lungs, kidney, liver, and spleen were collected and washed 3 times with Hank's Buffered Salt Solution (HBSS) and then cut into small pieces (around 2 to 3 mm) using a scalpel. After washing with HBSS, the pieces were transferred to light-protected disposable tubes containing HBSS and then placed on ice until used. In some experiments, adipose tissue pieces were subsequently stained with 5 μM of BODIPY493/503 (Invitrogen) and 20 μg/ml of Alexa647-GSIB4 for 1h to visualize adipocytes and blood vessels, respectively. The pieces that were transferred to glass-based dishes were viewed by confocal laser scanning microscopy (CLSM) (LSM-510; Carl Zeiss, or A1; Nikon). All images were recorded with sequential acquisition of the fluorescent channels.

2.5. Quantitative measurement of nanoparticles that had accumulated in tissues

After an *i.v*-injection of rhodamine-labeled NPs at several time points (5 or 24h), tissues (adipose or liver) from non-obese or obese mice were stained with a 20 μg/ml solution of Alexa647-GSIB4 for 1h and were observed by CLSM. All Z-series of images were exported as 8-bit TIFF-format image data and then transferred to the Image-Pro Plus software (Media Cybernetics Inc., Silver Spring, MD, USA). All of the stack files used as merged files was used to measure pixel area count, which satisfy the threshold pixel intensity in each RGB images or an arbitrary combination of RGB channels in a selected region. Digital noise was nullified by single-pixel signals.

2.6. Intracellular uptake of nanoparticles in vivo

Non-obese 6-wk-old male mice (C57BL/6J) were injected intravenously with PTNP or NTNP labeled with NBD-DOPE at the same lipid dose as described above. At 1h postinjection, the stromal vascular fraction (SVF) from inguinal regions was prepared as described previously [11]. After transferring the SVF to glass-base dishes, the samples were incubated for 2.5h at 37°C under an atmosphere with 5% CO_2. Cells that adhered to the bottom of the dishes were washed with heparin (40 U/ml) and incubated for a further 30 min under the same conditions with an addition of 2 ml EGM-2MV media (Lonza) and 5 μg/ml of Alexa647-GSIB4. Before the final washing, the cell nuclei were stained with Hoechst33342 (final conc. 2.5 μg/ml) and the cells were observed by CLSM.

2.7. Apoptosis assay in vivo

DIO mice (body weight >42g) remained untreated or received a single dose of KLA-PTNP and KLA-NTNP (1 mg/kg) or empty (E)-PTNP (0.2 mmol/kg) intravenously via the tail vein. At one day postinjection, the mice were killed by cervical dislocation, after which epididymal fat was removed and minced into small pieces. The tissue pieces were then washed and incubated with Alexa647-GSIB4 as described above. The tissues were then counterstained with a sulforhodamine-labeled FLICA (fluorescent-labeled inhibitors of caspase) Caspase 3 and 7 Assay Kit (Immunochemistry Technology).

2.8. Determination of vascular density

At 24h postinjection of E-PTNP, KLA-PTNP and KLA-NTNP to DIO mice, epididymal fat depots were removed from these and untreated mice and stained with Alexa647-GSIB4. The stained tissue pieces were then observed by CLSM with low magnification at z-stack mode. The isolectin-positive area (μm^2) was counted using Image J software (ver. 1.46) and then percentage of isolectin-positive area to the microscopic field area (μm^2) was calculated in each z-position. Among the percentages determined in each z-position of a z-stack image, the highest value was defined as the vascular density in the field. The mean vascular density was determined from 10-15 field images.

2.9. Anti-obesity study

The high-fat diet (HFD) (58Y1, 34.9% fat, 23.1% protein and 25.9% carbohydrates) and the normal diet (EQ 5L37, 4.5% fat, 25.0% protein and 49.3% carbohydrates) were purchased from the PMI Nutrition International (Richmond, IN, ISA). KLA-PTNP was prepared as described above. The Recovery Ratio of encapsulated KLA (9.4%) was taken into consideration in the dose calculation. DIO mice were allowed access to a HFD because this strain is prone to developing obesity throughout their lifespan. After the body weight reached around 44-45 g, we randomly divided the mice into 3 groups. Two groups of three mice per group were exposed to HFD along with an intravenous injection of 1 mg/kg of KLA-PTNP and KLA-NTNP at 3 day intervals for 30 days whereas the other group (n=3) remained untreated as a non-treated control. Mouse body weight was measured at 3 day intervals during therapy.

2.10. Statistical analysis

All statistical analyses were performed using the JMP6 statistical package (SAS Institute). One-way ANOVA followed by Dunnett's multiple comparison and Tukey-Kramer's HSD test was used to evaluate statistical significance. The paired *t*-test was also used to determine the statistical significance of each treatment on body weight. A p value of < 0.05 was considered to be significant.

3. Results

3.1. In vivo targeted delivery of ligand modified NPs to white fat vessels in normal mice

We first attempted to optimize the active targeting activity of the targeted-NPs for *in vivo* applications in normal healthy mice. On the basis of prototype NP (Pep-PEG_{2kDa}-NP) [10], we

additionally designed and prepared two other types of targeted NPs. One was Pep-PEG_{5kDa}-NP modified with the same ligand via a longer PEG spacer, while the other was prohibitin-targeted nanoparticle (PTNP) to which PEG_{2kDa} was further added to the surface of the Pep-PEG_{5kDa}-NP (**Fig. 1A**). Systemic administration of these three types of NPs labeled with rhodamine showed that PTNP accumulated in the blood vessels in subcutaneous adipose tissue (SAT) of normal mice at levels that were around 4.5- and 3.5-fold higher compared to those of Pep-PEG_{5kDa}-NP and Pep-PEG_{2kDa}-NP respectively, while showing a decrease in liver accumulation of around 39- and 7-fold (**Fig. 1B and C**). No consistent observable accumulation of PTNP was detected in brain, lung and kidney (**Fig. S2**). To further verify this finding as strong evidence, we directly compared the targeting activity of PTNP to either Pep-PEG_{5kDa}-NP or Pep-PEG_{2kDa}-NP by *i.v*-injection. PTNP showed a broader distribution on WFV compared with either Pep-PEG_{5kDa}-NP or Pep-PEG_{2kDa}-NP (**Fig. 1D**). These results indicate that although these three types of NPs were modified with the same amount of ligand and showed similar physicochemical properties such as size and ζ-potential (**Table 1**), the PTNP system had the highest active targeting potency to WFV, while the off-targets were spared.

3.2. In vivo evaluation of PTNP as an active targeting drug carrier to WFV

To evaluate active internalization of PTNP system to vascular endothelial cells, we analyzed the stromal vascular fraction isolated from SAT after *i.v*-injection. **Fig. 2A** clearly demonstrated that NBD-labeled PTNP was selectively internalized by the GSIB4-stained cells (endothelial cells), whereas non-targeted nanoparticle (NTNP) comprised of same the PEG density to PTNP system, except only for the absence of a targeting ligand, was not.

We next examined whether PTNP delivers the encapsulated drug compounds to the targeted site by utilizing an aqueous phase marker (encapsulated rhodamine). As a result, it also allowed a specific higher accumulation of encapsulated rhodamine to WFV, whereas free rhodamine alone did not (**Fig. 2B**). In addition, the aqueous rhodamine delivered via PTNP was retained in the WFV for at least up to 72h after administration (**Fig. 2C**). These results demonstrate that the PTNP system has the potential to deliver the encapsulated drug to the endothelial cells of WFV for sustained long periods of time.

3.3. Acceleration of targeted delivery of PTNP to obese adipose vessels through the passive accumulation of NPs into angiogenic regions

In order to apply the PTNP system to obesity therapy, verification that PTNP targets WFV in obese animals is a critical issue. Thus, we next compared the accumulation of rhodamine-labeled PTNP and NTNP to adipose tissue in DIO mice by confocal-based observations. As a result, PTNP accumulated in WFV at high levels at 24h after *i.v*-injection (**Fig. 3A**). Surprisingly, NTNP, which was used as a negative control of PTNP, was also clearly detected, despite the absence of active targeting machinery (**Fig. 3A**). However, the fluorescence of PTNP was detected in both of cluster-like regions and capillary vessels, whereas that of NTNP was appeared limitedly in the clusters. Confocal observations with high magnification demonstrated that the fluorescent signals of PTNPs were highly co-localized with vessels, while a part of NTNPs was not co-localized with vessels (**Fig. 3B**). It is known that the sprouting of new blood vessels from the preexisting vasculature is coupled to new adipocyte formation in the cluster regions in obese adipose tissue [2]. In addition, it has been also reported that an increase in vascular permeability in obese visceral fat is a hallmark of inflammation [13]. Therefore, we hypothesized that the physical properties of obese adipose vessels might enhance the passive accumulation of sterically stabilized NPs such as PEGylated NPs.

To assess this hypothesis, we examined the accumulation of PEGylated NPs with different PEG densities (1 or 10 mol% of total lipids) in adipose tissue of normal and DIO mice. As a result, the low density PEGylated NPs showed a poor accumulation in both adipose tissues of

normal and DIO mice. In contrast, the high density PEGylated NPs accumulated at substantial levels around the clusters in DIO fat depots at 24h postinjection, whereas in normal adipose tissue, the extent of accumulation was much less (**Fig. 4A**). In addition, to test the feasibility of the system's PEG-density (2.25 mol% of total lipids) to be sufficient for the passive accumulation in obese fat, we prepared the NTNP system and administered into both DIO and normal mice. Confocal observation suggests that NTNP was also highly accumulated into the obese fat, compared to normal fat (**Fig. 4B**). Analyses of several images indicated that the total accumulation of NTNP in obese fat was 35-fold higher than that of normal fat (**Fig. 4C**) and it was appeared to be distributed as around 56% extravasated (outside of vessels) whereas that of NTNP in normal fat, around 5% NTNP had undergone extravasation (**Fig. 4D**). These results strongly support our hypothesis and also suggest that the accumulation of PTNP, which is equipped with active targeting machinery, into WFV of obese mice could be accelerated by the passive targeting mechanism.

Furthermore, fluorescent-labeled PTNP was not detected in other organs such as heart, brain, lung, kidney, liver and spleen at 5h after *i.v*-injection (**Fig. S3**).

3.4. Vascular-targeted nanotherapy of diet-induced obesity

For a pharmacological assessment, we selected the proapoptotic peptide (KLA) as a model compound and prepared E-PTNP, KLA-loaded PTNP (KLA-PTNP) and NTNP (KLA-NTNP). They were intravenously injected into DIO mice, and the induction of apoptosis in adipose tissue was then analyzed at 24h postinjection. As shown in **Fig. 5A**, KLA-PTNP treatment induced strong caspase activation GSIB4-positive cells, especially in the cluster regions. On the other hand, caspase activation was also observed in adipose tissue of KLA-NTNP treated mice, however, the apoptotic signals were poorly co-localized with vessels. In addition, we measured the average vessel density (percentages of GSIB4-positive area per unit area) in adipose tissue at 24h after the administration of E-PTNP, KLA-PTNP or NTNP by confocal-based observations. As a result, KLA-PTNP significantly reduced vessel density in adipose tissue, compared to other groups (**Fig. 5B**). These results were entirely consistent with their distribution in adipose tissue and might reflect the difference in targeted action on the adipose vasculature.

Next, the anti-obesity effect of KLA-PTNP and NTNP was examined. We treated DIO mice at 3 day intervals for a total of 18 days by the *i.v*-injections of KLA-PTNP and NTNP at a dose of 1 mg/kg, respectively. The weight gain of the non-treated (NT) mice was accelerated by feeding a high-fat diet, whereas weight gain for both KLA-PTNP and KLA-NTNP treated mice was significantly less than that of the NT group (**Fig. 5C**). On day 18 of the treatment period, the body weight of KLA-PTNP treated mice was significantly less than their initial weight (5% reduction). On the contrary, that of KLA-NTNP treated mice was significantly higher than their initial (8% increase) (**Table 2**). These results indicate that the targeted disruption of blood vessels in adipose tissue effectively leads to a reduction in body weight in DIO mice. Collectively, these data clearly demonstrate that the higher therapeutic effects of vascular-targeted nanotherapy are mediated by the enhanced delivery of drugs to the target site via dual mechanisms, i.e., both passive and active targeting (**Fig. 6**).

4. Discussion

In the present study, we demonstrated, for the first time, that the targeted delivery of drugs to adipose endothelial cells via a nanoparticle-based system was substantially promoted by a physical property (enhanced permeability) of a discontinuous architecture in angiogenic vessels. In addition, the systemic administration of prohibitin-targeted nanoparticles (PTNP), in which proapoptotic agents were incorporated, significantly suppressed the progression of diet-induced obesity in mice.

We recently reported on the development of an *in vitro* adipose endothelial cell targeting nanoparticle [10]. The prototype NP was a liposomal nanocarrier modified with a targeting motif (KGGRAKD) [6] via a PEG_{2kDa} spacer (Pep-PEG_{2kDa}-NP). For *in vivo* applications, we additionally designed two other types of targeted NPs (Pep-PEG_{5kDa}-NP and PTNP) and compared the delivery of these three types of NPs into WFV in normal healthy mice by confocal-based observations. Although these three types of NPs were modified with the same amount of ligand and showed similar physicochemical properties, including size and ζ-potential (**Table 1**), their targeting activities were substantially different after systemic injection. It was reported that a longer PEG spacer has the benefit of the flexibility to exclude steric hindrance for recognition to the targeted receptors that may increase ligand-receptor interactions [14]. However, in our examination, a significant increase in the undesirable accumulation of Pep-PEG_{5kDa}-NPs in the liver was found, and no improvement in the targeted delivery to WFV was observed, compared to that of the prototype Pep-PEG_{2kDa}-NPs (**Fig. 1B and C**). Generally, PEGylation is a useful strategy for avoiding the recognition of NP by the reticuloendothelial system (RES) because if forms a hydrophilic layer around the carrier [15, 16]. PTNP is a PEGylated form of Pep-PEG_{5kDa}-NP, prepared using a PEG_{2kDa} polymer, and hence, showed a significantly lower accumulation in the liver than Pep-PEG_{5kDa}-NP. In addition to reduced entrapment in the liver, the accumulation in WFV of PTNP was around 4-fold higher compared to the corresponding values for Pep-PEG_{5kDa}-NP and Pep-PEG_{2kDa}-NP (**Fig. 1B and C**). The direct comparison of the targeted delivery between PTNP and the other two types of NPs also demonstrated the similar results (**Fig. 1D**). These results clearly indicate that the *in vivo* targeting activity of NPs equipped with targeting machinery does not completely depend on the binding affinity of a ligand to its receptor. In this study, we demonstrated that the enhanced targeting activity of PTNP was mediated by co-modification with Pep-PEG_{5kDa} and PEG_{2kDa}, however, further investigations will be needed to determine the detailed molecular basis.

We confirmed the active targeting potency of PTNP by confocal observations, which showed that PTNP was taken up by the vascular endothelial cells of adipose tissue after *i.v*-injection to normal mice whereas NTNP did not (**Fig. 2A**). In addition, the long-time retention of PTNP in WFV was also validated (**Fig. 2C**). We previously reported that targeted NPs modified with a WFV-homing peptide were taken up by the vascular endothelial cells isolated from murine adipose tissue via prohibitin-mediated endocytosis and this might allow them to escape from lysosomal degradation [10]. Though the detailed mechanism for the intracellular trafficking of NPs in endothelial cells remains unclear, the higher accumulation of PTNP in a sustained-releasing manner to the WFV might be advantageous for the design of a low dosage-regimen in clinical applications.

Previously, Kolonin *et al*. originally identified the prohibitin-targeted peptide motif by *in vivo* phage display using a mouse model of genetic obesity ($Lep^{ob/ob}$) [6]. In a previous report, they also showed the homing of the peptide to WFV in non-obese wild-type mice. Therefore, it was assumed that PTNP also accumulates into WFV in DIO mice as well as in normal mice. In fact, as in normal mice, PTNP accumulated substantially in WFV in DIO mice (**Fig. 3A**). In this evaluation, we found an extensive accumulation of NTNP, which was used as a negative control, in obese fat despite the absence of active targeting machinery (**Fig. 3A**). As described above, NTNP is not recognized and is not taken up by the vascular endothelial cells of adipose tissue in normal mice, hence, the unexpected accumulation of NTNP in obese adipose tissue might be mediated by a passive mechanism. Actually, NTNP accumulation occurs in cluster-like regions, whilst it was negligible in capillary vessels. It is known that the sprouting of new blood vessels from the preexisting vasculature is coupled to new adipocyte formation in cluster regions in obese adipose tissue [2]. Furthermore, it was also reported that an increase in vascular permeability in obese visceral fat is a hallmark of inflammation [13].

Therefore, the accumulation of NTNP in the clusters of obese adipose tissue may be the result of the physical properties of the neovasculature, which possesses a discontinuous architecture and enhanced permeability, and the nanoscaled properties of drug carriers. Namely, it could be mediated by a mechanism similar to that for the well known enhanced permeability and retention (EPR)-effect associated with tumor targeting [17]. Confocal observations and image analyses clearly demonstrated the permeation of NTNP into intercellular space, although PTNP highly co-localized with vessels (**Fig. 3B** and **4**). These findings provide strong support for our hypothesis. Therefore, the multivalent active recognition of PTNP by vascular endothelial cells in white fat via a specific ligand might be co-enhanced by the passive accumulation around clusters, due to its nanosized properties.

An *in vivo* apoptosis assay demonstrated that KLA-loaded PTNP strongly induced caspase activation in isolectin-positive cells of the clusters in obese fat, whereas KLA-NTNP showed marginal effects in isolectin-negative regions, compared to NT and E-PTNP (**Fig. 5A**). In addition, vascular density in adipose tissue, which was measured as the isolectin-positive area per unit area, was significantly lower in KLA-PTNP treated mice, compared to other groups (**Fig. 5B**). These results may be reasonable, since it has been previously reported that the KLA peptide itself was not internalized by cells and required an appropriate intracellular delivery strategy to induce apoptosis [18]. We also demonstrated that the vascular-targeted delivery of the KLA peptide via PTNP significantly suppressed the progression of obesity caused by feeding of high-fat diet (**Fig. 5C**). Although the body weight in each group was similar at the initial day of treatment, the mean body weight in KLA-PTNP treated mice was around 15% lower than that in NT mice after 18 days of treatment (**Table 2**). This result clearly indicates that vascular-targeted nanotherapy integrating antiangiogenesis with nanotechnology is highly promising strategy for effective control of obesity. Moreover, the ligand receptor prohibitin was also expressed in human WFV [19]. Therefore, this work may, in the near future, offer a paradigm shift in the discovery and development of anti-obesity drugs for the treatment of human obesity.

5. Conclusion

The findings presented herein show that the PEGylation of targeted NPs, modified with a WFV-homing ligand, can reduce undesired entrapment in liver and hence, improve the efficient targeting to adipose vessels. In addition, the findings also indicate that NPs are sterically stabilized by a hydrophilic polymer such as PEG and accumulate passively in angiogenic clusters in obese white fat. Although passive drug targeting mediated by the EPR-effect has been accepted as the gold standard in drug design for anti-tumor agents, no evidence of passive drug targeting via the EPR-like mechanism in obese fat has been reported to date. The PTNP system, which is modified with both an active targeting motif via a PEG linker and a hydrophilic PEG polymer, has the ability to specifically deliver encapsulated therapeutics to adipose endothelial cells *in vivo*, and the targeted delivery of PTNP could be further enhanced by the architectural properties of the angiogenic vasculature in adipose tissue when it is administered to obese animals. The findings that the systemic administration of the proapoptotic peptide, used as a model drug, via PTNP significantly suppressed the body weight gain of DIO mice as a result of the targeted disruption of the adipose vasculature provide a proof-of-concept for adipose endothelial cell-targeted nanotherapy in obesity that integrates antiangiogenesis with nanotechnology.

Acknowledgments

This study was supported by grants from the Special Education and Research Expenses of the Ministry of Education, Culture, Sports, Science and Technology of Japan. We thank Dr. Milton Feather for editing this manuscript.

References

[1] A. Bouloumie, K. Lolmede, C. Sengenes, J. Galitzky, M. Lafontan, Angiogenesis in adipose tissue, Ann Endocrinol (Paris), 63 (2002) 91-95.

[2] S. Nishimura, I. Manabe, M. Nagasaki, Y. Hosoya, H. Yamashita, H. Fujita, M. Ohsugi, K. Tobe, T. Kadowaki, R. Nagai, S. Sugiura, Adipogenesis in obesity requires close interplay between differentiating adipocytes, stromal cells, and blood vessels, Diabetes, 56 (2007) 1517-1526.

[3] M.A. Rupnick, D. Panigrahy, C.Y. Zhang, S.M. Dallabrida, B.B. Lowell, R. Langer, M.J. Folkman, Adipose tissue mass can be regulated through the vasculature, Proc Natl Acad Sci U S A, 99 (2002) 10730-10735.

[4] E. Brakenhielm, R. Cao, B. Gao, B. Angelin, B. Cannon, P. Parini, Y. Cao, Angiogenesis inhibitor, TNP-470, prevents diet-induced and genetic obesity in mice, Circ Res, 94 (2004) 1579-1588.

[5] R. Satchi-Fainaro, M. Puder, J.W. Davies, H.T. Tran, D.A. Sampson, A.K. Greene, G. Corfas, J. Folkman, Targeting angiogenesis with a conjugate of HPMA copolymer and TNP-470, Nat Med, 10 (2004) 255-261.

[6] M.G. Kolonin, P.K. Saha, L. Chan, R. Pasqualini, W. Arap, Reversal of obesity by targeted ablation of adipose tissue, Nat Med, 10 (2004) 625-632.

[7] H.M. Ellerby, W. Arap, L.M. Ellerby, R. Kain, R. Andrusiak, G.D. Rio, S. Krajewski, C.R. Lombardo, R. Rao, E. Ruoslahti, D.E. Bredesen, R. Pasqualini, Anti-cancer activity of targeted pro-apoptotic peptides, Nat Med, 5 (1999) 1032-1038.

[8] K.F. Barnhart, D.R. Christianson, P.W. Hanley, W.H. Driessen, B.J. Bernacky, W.B. Baze, S. Wen, M. Tian, J. Ma, M.G. Kolonin, P.K. Saha, K.A. Do, J.F. Hulvat, J.G. Gelovani, L. Chan, W. Arap, R. Pasqualini, A peptidomimetic targeting white fat causes weight loss and improved insulin resistance in obese monkeys, Sci Transl Med, 3 (2011) 108ra112.

[9] D.H. Kim, S.C. Woods, R.J. Seeley, Peptide designed to elicit apoptosis in adipose tissue endothelium reduces food intake and body weight, Diabetes, 59 (2010) 907-915.

[10] M.N. Hossen, K. Kajimoto, H. Akita, M. Hyodo, T. Ishitsuka, H. Harashima, Ligand-based targeted delivery of a peptide modified nanocarrier to endothelial cells in adipose tissue, J Control Release, 147 (2010) 261-268.

[11] K. Kajimoto, M.N. Hossen, K. Hida, N. Ohga, H. Akita, M. Hyodo, Y. Hida, H. Harashima, Isolation and culture of microvascular endothelial cells from murine inguinal and epididymal adipose tissues, J Immunol Methods, 357 (2010) 43-50.

[12] F. Szoka, Jr., D. Papahadjopoulos, Procedure for preparation of liposomes with large internal aqueous space and high capture by reverse-phase evaporation, Proc Natl Acad Sci U S A, 75 (1978) 4194-4198.

[13] S. Nishimura, I. Manabe, M. Nagasaki, K. Seo, H. Yamashita, Y. Hosoya, M. Ohsugi, K. Tobe, T. Kadowaki, R. Nagai, S. Sugiura, In vivo imaging in mice reveals local cell dynamics and inflammation in obese adipose tissue, J Clin Invest, 118 (2008) 710-721.

[14] A. Gabizon, A.T. Horowitz, D. Goren, D. Tzemach, H. Shmeeda, S. Zalipsky, In vivo fate of folate-targeted polyethylene-glycol liposomes in tumor-bearing mice, Clin Cancer Res, 9 (2003) 6551-6559.

[15] W.Y. Ayen, B. Chintankumar, J.P. Jain, N. Kumar, Effect of PEG chain length and hydrophilic weight fraction on polymersomes prepared from branched (PEG)(3)-PLA co-polymers, Polym Advan Technol, 22 (2011) 158-165.

[16] H. Hatakeyama, H. Akita, H. Harashima, A multifunctional envelope type nano device (MEND) for gene delivery to tumours based on the EPR effect: a strategy for overcoming the PEG dilemma, Adv Drug Deliv Rev, 63 (2011) 152-160.

[17] Y. Matsumura, H. Maeda, A new concept for macromolecular therapeutics in cancer chemotherapy: mechanism of tumoritropic accumulation of proteins and the antitumor agent smancs, Cancer Res, 46 (1986) 6387-6392.
[18] K. Karjalainen, D.E. Jaalouk, C.E. Bueso-Ramos, A.J. Zurita, A. Kuniyasu, B.L. Eckhardt, F.C. Marini, B. Lichtiger, S. O'Brien, H.M. Kantarjian, J.E. Cortes, E. Koivunen, W. Arap, R. Pasqualini, Targeting neuropilin-1 in human leukemia and lymphoma, Blood, 117 (2011) 920-927.
[19] F.I. Staquicini, M. Cardo-Vila, M.G. Kolonin, M. Trepel, J.K. Edwards, D.N. Nunes, A. Sergeeva, E. Efstathiou, J. Sun, N.F. Almeida, S.M. Tu, G.H. Botz, M.J. Wallace, D.J. O'Connell, S. Krajewski, J.E. Gershenwald, J.J. Molldrem, A.L. Flamm, E. Koivunen, R.D. Pentz, E. Dias-Neto, J.C. Setubal, D.J. Cahill, P. Troncoso, K.A. Do, C.J. Logothetis, R.L. Sidman, R. Pasqualini, W. Arap, Vascular ligand-receptor mapping by direct combinatorial selection in cancer patients, Proc Natl Acad Sci U S A, 108 (2011) 18637-18642.

Figure legends

Fig. 1. *In vivo* targeted delivery of nanocarriers to white fat vessels in normal mice

(**A**) Schematic illustration of the design of vascular-targeted NPs. PTNP indicates prohibitin-targeted nanoparticle. (**B**) Comparison of targeted and off-targeted accumulation of NPs. Normal mice were *i.v*-injected with rhodamine-labeled Pep-PEG_{2kDa}-NP, Pep-PEG_{5kDa}-NP or PTNP (red). To visualize blood vessels, 50 μg of FITC-GSIB4 (green) was also *i.v*-injected 30 min prior to tissue processing. At 5h after administration, the subcutaneous adipose tissue (SAT) and liver were imaged by CLSM. (**C**) Quantification of nanoparticles into WFV and liver. Red fluorescence of NPs accumulated in SAT and liver was normalized to the green fluorescence of blood vessels for quantification. Data represent the mean ± SD (n=3); †P<0.005 (One-way ANOVA followed by Tukey-Kramer's HSD test). (**D**) Direct comparison of targeted delivery between PTNP and the other two types of NPs. Mice were *i.v*-injected with the mixture of NP labeled by different fluorescent dyes (rhodamine-labeled PTNP (red) and NBD-labeled Pep-PEG_{2kDa}- or Pep-PEG_{5kDa}-NP (green)). To visualize blood vessels, 50 μg of Alexa647-GSIB4 (cyan) was also *i.v*-injected 30 min prior to tissue processing. At 5h after *i.v*-injection, SAT was imaged by CLSM. Bars represent 100 μm (B and D).

Fig. 2. *In vivo* evaluation of the potential of PTNP in normal mice

(**A**) *In vivo* uptake of NPs into vascular endothelial cells of adipose tissue. Normal mice were *i.v*-injected with NBD-labeled PTNP and NTNP (green). At 1h after injection, the stromal-vascular cell fractions were collected from SAT and seeded onto grass-based dishes. The vascular endothelial cells were visualized with Alexa647-GSIB4 (red). Nuclei were also counterstained by Hoechst33342 (blue). (**B**) Delivery of aqueous phase marker into WFV by PTNP. Rhodamine-loaded PTNP and free rhodamine solution (red) at the same dose were injected intravenously. Vessel visualization (green) was performed as described above. At 24h after injection, SAT was observed by CLSM. (**C**) Long-term retention of PTNP in WFV. Mice were intravenously injected with rhodamine-loaded PTNP (red). At 24, 48 and 72h after administration, SAT was viewed with CLSM. The blood vessels were visualized by FITC-GSIB4 (green) injection as described above. Scale bars represent 20 μm (A) and 100 μm (B and C).

Fig. 3. Enhanced targeting of PTNP to WFV enhanced by active and passive mechanism in DIO mice

(**A**) *In vivo* accumulation of PTNP and NTNP into WFV in DIO mice. DIO mice were intravenously injected with rhodamine-loaded PTNP and NTNP (green) at the same rhodamine dose (0.2 μmol/kg). At 5h after injection, EAT pieces were stained with

Alexa647-GSIB4 (red). (**B**) Confocal observation of angiogenic clusters with high-magnification. At 5h after injection of rhodamine-loaded PTNP or NTNP (green) as mentioned above, EAT pieces were stained with Alexa647-GSIB4 (red) and BODIPY493/503 (Blue). Scale bars represent 100 μm (A) and 20 μm (B).

Fig. 4. Passive accumulation of PEGylated NPs into the angiogenic clusters in obese fat
The normal and DIO mice were *i.v*-injected with fluorescent-labeled PEGylated-NP (1 or 10 mol% of total lipids) (green). At 24h after injection, EAT pieces were stained with Alexa647-GSIB4 (red). (**B**) Confocal observation of NTNP in the EAT of normal and DIO mice. Normal and DIO mice were intravenously injected with rhodamine-labeled NTNP (green) at a total lipid dose of 0.1 mmol/kg. At 24h after injection, portions of EAT tissue from both mice were also stained with Alexa647-GSIB4 (red) and were observed by CLSM. (**C** and **D**) Measurement of the accumulated NTNP in the EAT of normal and DIO mice. Images data (n=5) were allowed to measure pixel area count and expressed as the total fluorescent signals detected in unit area (C) and the percentages of the extravasated to total rhodamine signals (D). Data represents the mean ± SD; #P<0.0001 (Student's t-test). Bars are 100 μm.

Fig. 5. Suppression of obesity through KLA-PTNP mediated by targeted disruption of adipose vasculature
(**A**) *In vivo* apoptosis assay. DIO mice were intravenously injected with KLA-PTNP and KLA-NTNP (1 mg/kg) and empty (E)-PTNP (0.2 mmol/kg) or remained untreated (NT). At 24h after injection, the EAT specimens were stained with an apoptosis detection reagent (green) and Alexa647-GSIB4 (red). Bars represent 100 μm. (**B**) Measurement of vascular density. At 24h after injection of KLA-PTNP, KLA-NTNP, E-PTNP and NT, the mean percentages of isolectin-positive area in microscopic field area in EAT pieces were determined as the vascular density. (**C**) Body weight gain in response to treatment. DIO mice (n=3) exposed to a high fat diet were intravenously injected with KLA-PTNP and KLA-NTNP (1 mg/kg) or non-treated (NT) at 3 day intervals for 18 days. Mouse body weight was measured every 3 days. Percentages of body mass of mice to their initial weights were determined. Statistical analyses were performed with Student's t-test in (B) and one-way ANOVA followed by Tukey-Kramer's HSD test in (C). Data represents the mean ± SD; #P<0.0001 and *P<0.05.

Fig. 6. Dual mechanism of enhanced drug delivery caused by passive and active targeting of PTNP into obese adipose tissue
(**A**) A confocal image of angiogenic/adipogenic cell clusters in obese adipose tissue. The cluster consists of immature adipocyte (blue) that is surrounded by proliferating endothelial cells (red), which are the precursors for the formation of the capillary vessels, and other stromal cells, as indicated by staining with all cell nuclei (green). Obese adipose tissue also contains both hypertrophied adipocytes (blue) and capillary vessels (red) between the adipocytes. Scale bars represent 100 μm. (**B**) Graphical illustration of dual mechanisms for passive and active targeting by which intravenously administered PTNP accumulates into endothelial cells of obese adipose tissue. PTNP system passively accumulates into the angiogenic space through both the abnormal vascular architecture and its nanosized properties (red arrows). Subsequently, the multivalent active recognition and uptake of PTNP system by endothelial cells may occur via the ligand-receptor interaction (blue arrows).

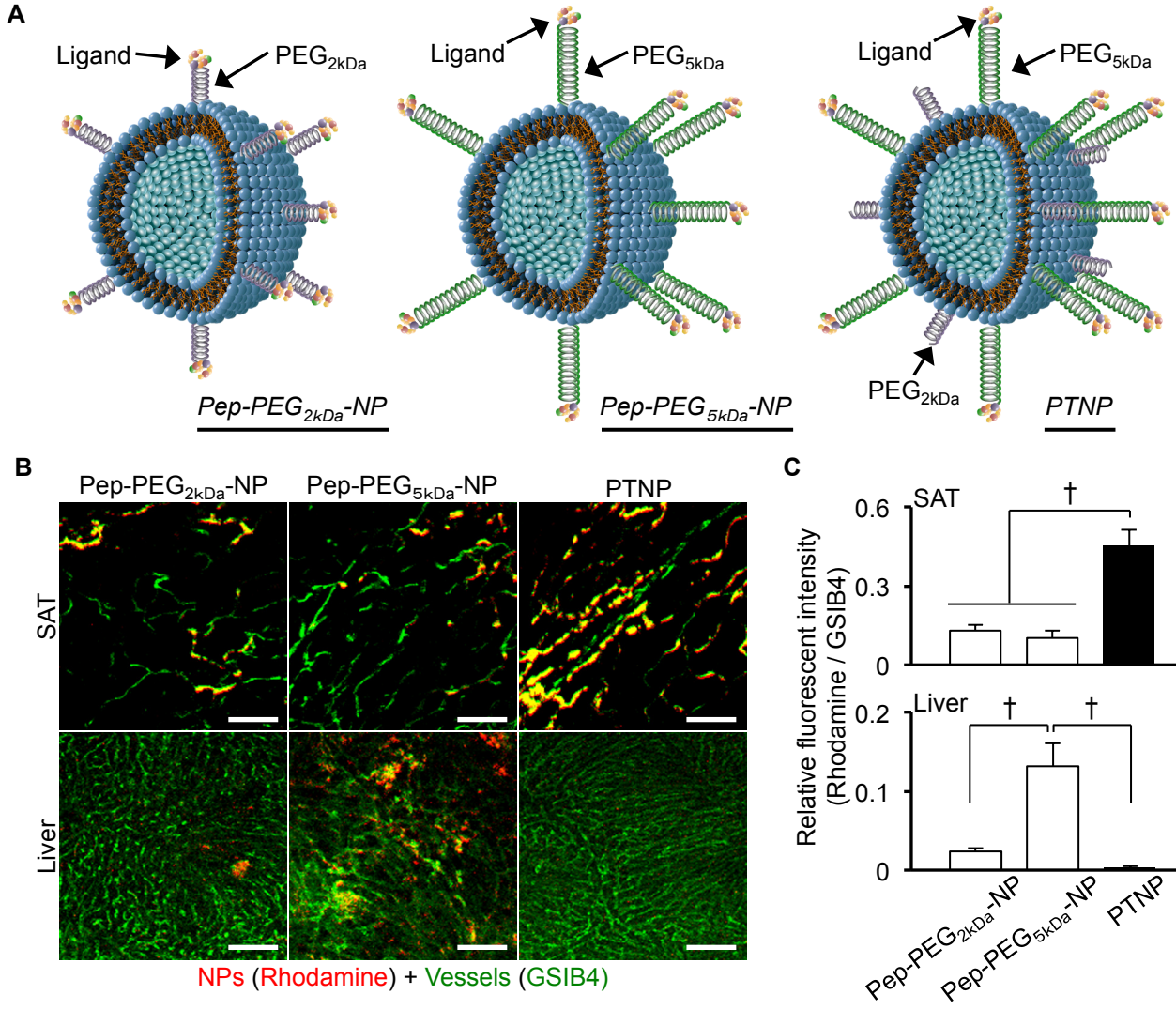
A
Ligand
PEG2kDa
Pep-PEG2kDa-NP
Ligand
PEG5kDa
Pep-PEG5kDa-NP
Ligand
PEG5kDa
PEG2kDa
PTNP
B
Pep-PEG2kDa-NP
Pep-PEG5kDa-NP
PTNP
SAT
Liver
NPs (Rhodamine) + Vessels (GSIB4)
C
SAT
Liver
Relative fluorescent intensity (Rhodamine / GSIB4)
0.6
0.3
0
0.2
0.1
0
†
†
†
Pep-PEG2kDa-NP
Pep-PEG5kDa-NP
PTNP
D
Merged (Green & Red)
Pep-PEG2kDa
PTNP
Vessels
Merged (Green & Red)
Pep-PEG5kDa
PTNP
Vessels
NPs (NBD) + PTNP (Rhodamine) + Vessels (GSIB4)

Figure 1

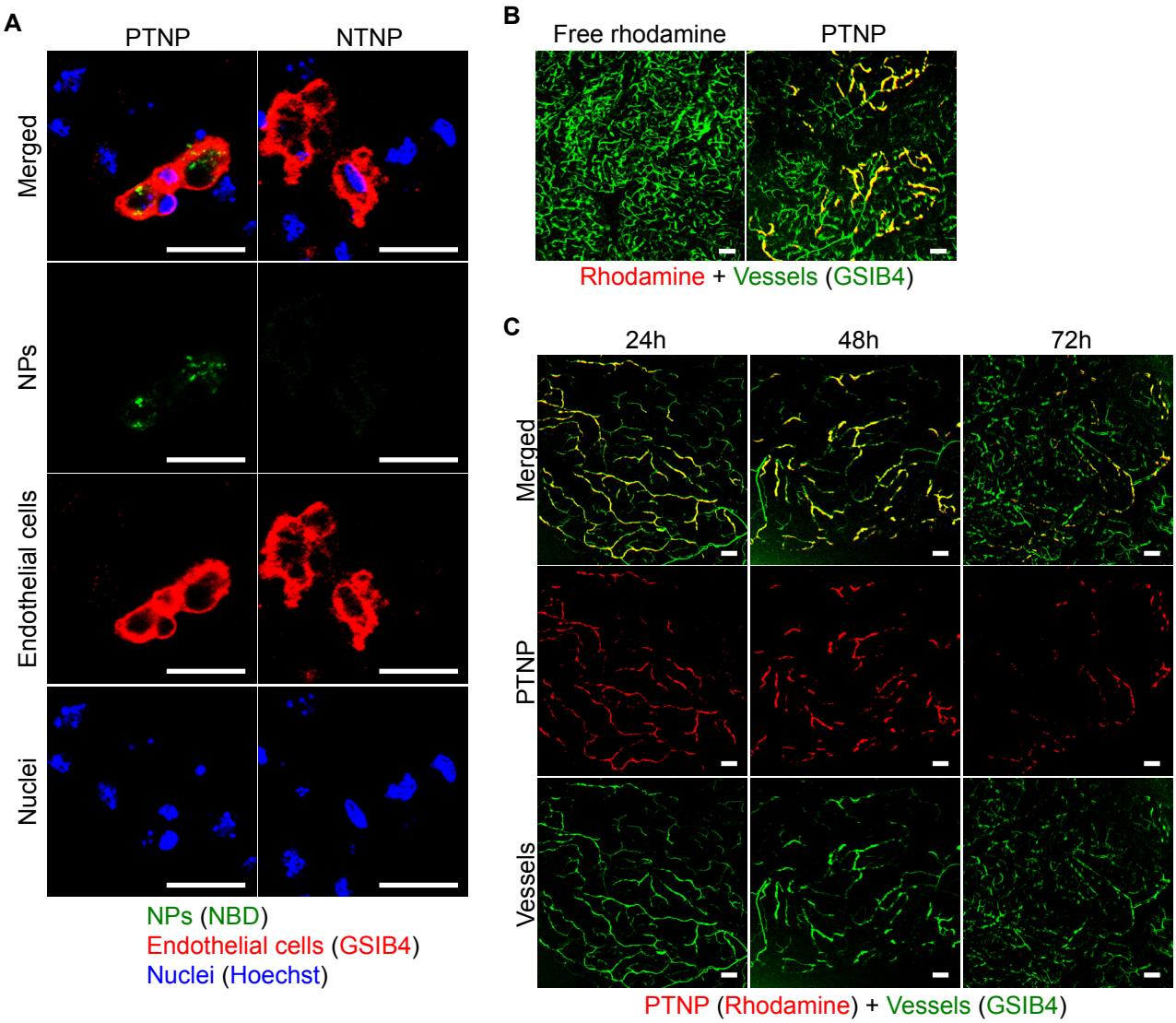
A
PTNP
NTNP
Merged
NPs
Endothelial cells
Nuclei
NPs (NBD)
Endothelial cells (GSIB4)
Nuclei (Hoechst)
B
Free rhodamine
PTNP
Rhodamine + Vessels (GSIB4)
C
24h
48h
72h
Merged
PTNP
Vessels
PTNP (Rhodamine) + Vessels (GSIB4)

Figure 2

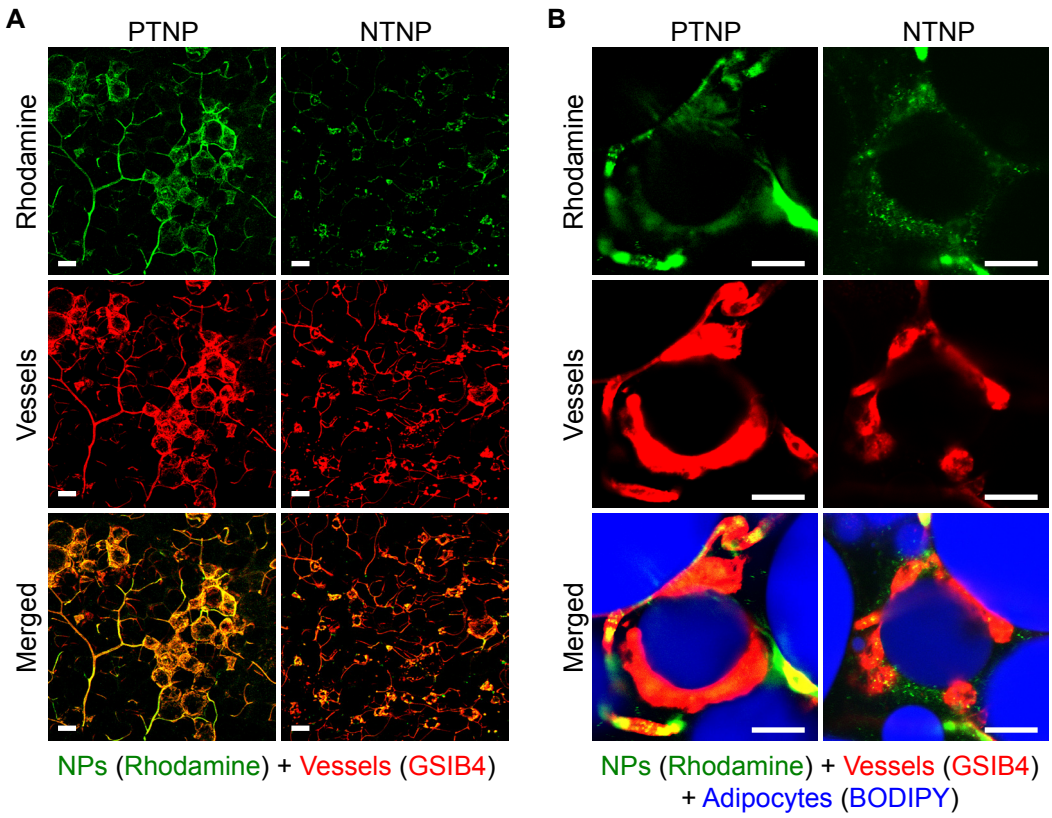
A
PTNP
NTNP
Rhodamine
Vessels
Merged
NPs (Rhodamine) + Vessels (GSIB4)
B
PTNP
NTNP
Rhodamine
Vessels
Merged
NPs (Rhodamine) + Vessels (GSIB4)
+ Adipocytes (BODIPY)

Figure 3

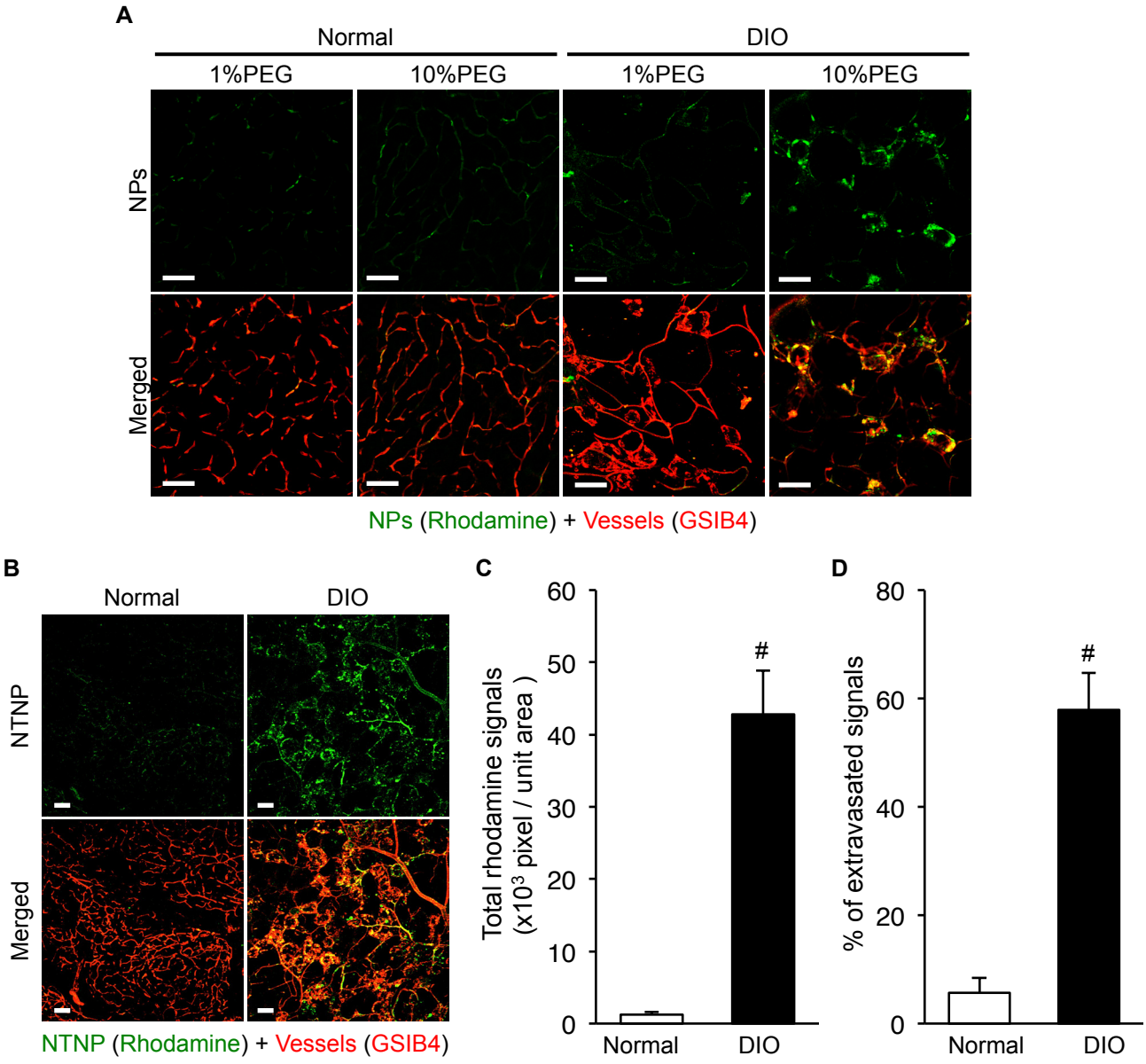
A
Normal
DIO
1%PEG
10%PEG
1%PEG
10%PEG
NPs
Merged
NPs (Rhodamine) + Vessels (GSIB4)
B
Normal
DIO
NTNP
Merged
NTNP (Rhodamine) + Vessels (GSIB4)
C
Total rhodamine signals
(x10³ pixel / unit area)
60
50
40
30
20
10
0
#
Normal
DIO
D
% of extravasated signals
80
60
40
20
0
#
Normal
DIO

Figure 4

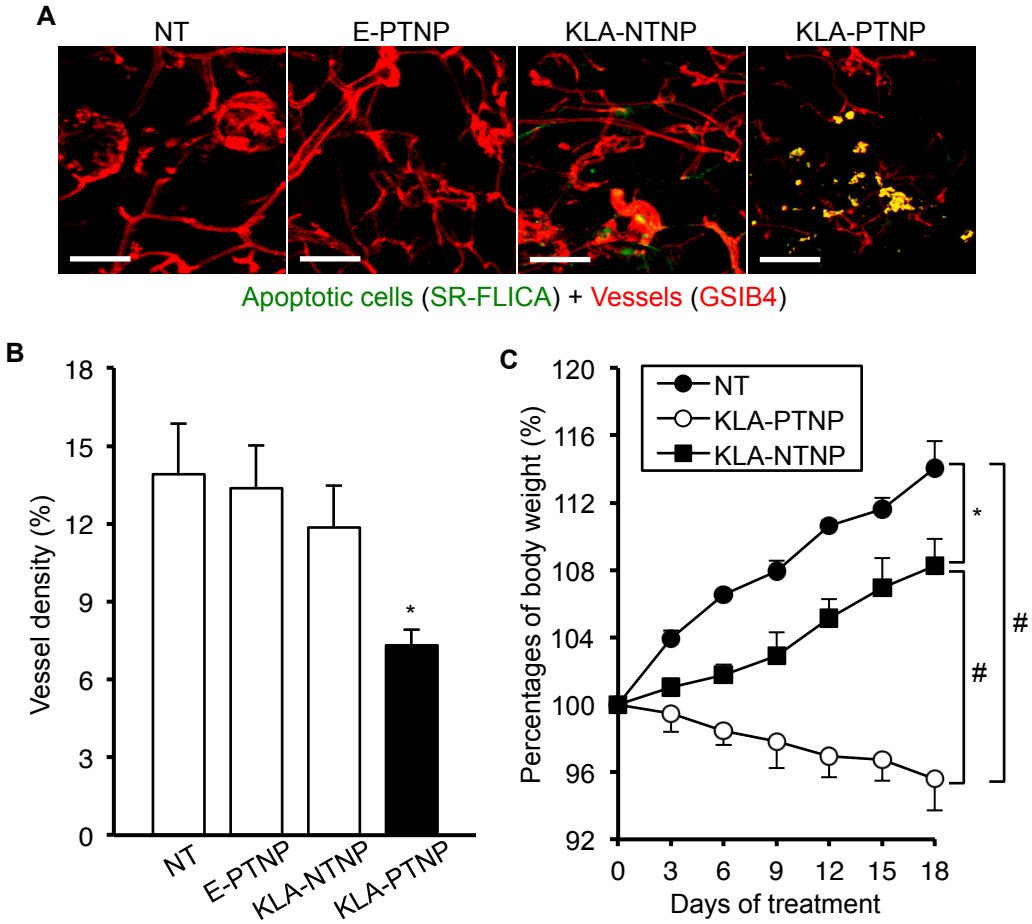
A
NT
E-PTNP
KLA-NTNP
KLA-PTNP
Apoptotic cells (SR-FLICA) + Vessels (GSIB4)
B
Vessel density (%)
18
15
12
9
6
3
0
*
NT
E-PTNP
KLA-NTNP
KLA-PTNP
C
Percentages of body weight (%)
120
116
112
108
104
100
96
92
NT
KLA-PTNP
KLA-NTNP
*
#
#
0
3
6
9
12
15
18
Days of treatment

Figure 5

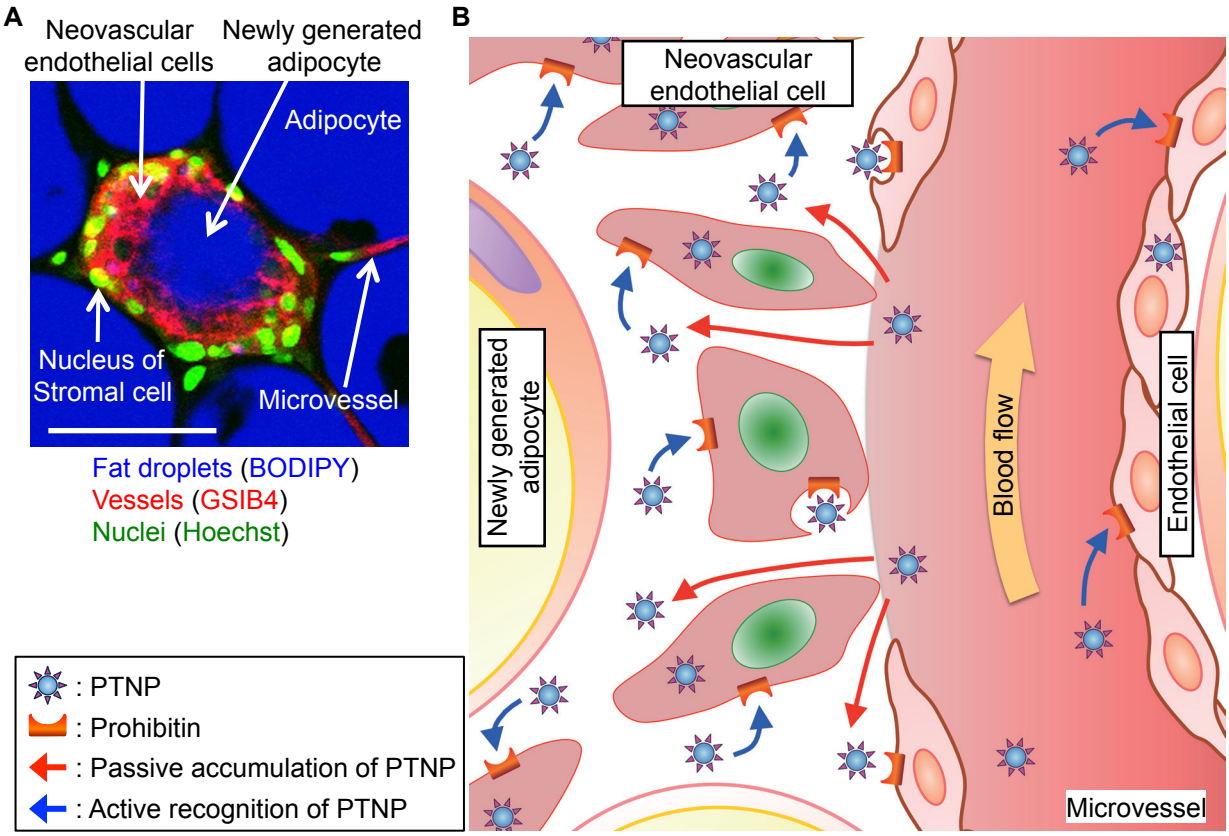
A
Neovascular endothelial cells
Newly generated adipocyte
Adipocyte
Nucleus of Stromal cell
Microvessel
Fat droplets (BODIPY)
Vessels (GSIB4)
Nuclei (Hoechst)
: PTNP
: Prohibitin
: Passive accumulation of PTNP
: Active recognition of PTNP
B
Neovascular endothelial cell
Newly generated adipocyte
Blood flow
Endothelial cell
Microvessel

Figure 6

Tables

Table 1. Physicochemical properties of nanoparticles.

Encapsulated compounds	NPs	Average size (nm)	ζ-potential (mV)
Empty	Pep-PEG_{2kDa}-NP	111.8 ± 7.9	-0.04 ± 3.4
	Pep-PEG_{5kDa}-NP	116.9 ± 5.5	-0.26 ± 1.8
	PTNP	116.0 ± 9.0	-3.37 ± 2.7
	NTNP	100.5 ± 1.5	-14.0 ± 0.8
$_D(KLAKLAK)_2$	PTNP	109.2 ± 7.8	6.0 ± 0.9
	NTNP	133.5 ± 6.9	-5.7 ± 0.9
Rhodamine	PTNP	105.5 ± 3.1	-4.0 ± 0.3
	NTNP	108.1 ± 6.1	-14.4 ± 1.7
	1% PEG-NP	111.6 ± 3.6	-8.6 ± 0.7
	10% PEG-NP	105.3 ± 5.6	-21.4 ± 2.9

Nanoparticles were prepared by the reverse phase evaporation (REV) method. The sizes and zeta potentials of them were measured by means of a Malvern Zetasizer. Data are represented as the mean ± SD of at least three independent preparations.

Table 2. Average body weight of mice before and after treatment.

Group	Body weight (g)		*p*-value of paired *t*-test
	Before	After	
NT	44.3 ± 2.5	50.5 ± 2.2	0.0011
KLA-PTNP	45.2 ± 2.7	43.2 ± 3.3	0.0483
KLA-NTNP	44.8 ± 2.4	48.5 ± 2.0	0.0082

Data are the mean ± SD of 3 mice in each group. The paired *t*-test was performed to determine the differences between before and after treatment.